Magnetic structures of $R_3Mn_4Sn_4$ (R = La, Pr and Nd)

2003 J. Phys.: Condens. Matter 15 803

(http://iopscience.iop.org/0953-8984/15/6/307)

INSTITUTE OF PHYSICS PUBLISHING JOURNAL OF PHYSICS: CONDENSED MATTER

J. Phys.: Condens. Matter **15** (2003) 803–814 PII: S0953-8984(03)39316-6

Magnetic structures of $R_3Mn_4Sn_4$ (R = La, Pr and Nd)

E Wawrzyńska[1], S Baran[1], J Leciejewicz[2], W Sikora[3], N Stüsser[4] and A Szytuła[1]

[1] M Smoluchowski Institute of Physics, Jagiellonian University, Reymonta 4, 30-059 Kraków, Poland
[2] Institute of Nuclear Chemistry and Technology, Dorodna 16, 03-169 Warszawa, Poland
[3] Faculty of Physics and Nuclear Techniques, Academy of Mining and Metallurgy, Reymonta 19, 30-059 Kraków, Poland
[4] BENSC, Hahn-Meitner Institut, Glienicker Straße 100, D-14109 Berlin-Wannsee, Germany

E-mail: wawrzyn@castor.if.uj.edu.pl

Received 10 July 2002, in final form 18 December 2002
Published 3 February 2003
Online at stacks.iop.org/JPhysCM/15/803

Abstract

Neutron diffraction studies of polycrystalline $R_3Mn_4Sn_4$ (R = La, Pr, Nd) intermetallic compounds with the orthorhombic $Gd_3Cu_4Ge_4$-type crystal structure indicate the existence of different magnetic structures. The magnetic structures were studied with the support of group theoretical considerations. For R = La a sine wave modulated structure described by the propagation vector $\boldsymbol{k} = (k_x, 0, 0)$ is observed below $T_N = 300$ K. This ordering is stable down to 1.5 K. For the $Pr_3Mn_4Sn_4$ and $Nd_3Mn_4Sn_4$ compounds the Mn moments form a non-collinear antiferromagnetic structure below the Néel temperatures of 230 and 210 K, respectively. Below $T_t = 25$ and 60 K for R = Pr and Nd, respectively, the rare earth Pr and Nd moments also order and form collinear magnetic structures while the magnetic order of the Mn moments remains unchanged.

1. Introduction

The investigation presented in this paper is a part of a more complete study, which is expected to systematize the magnetic properties—including magnetic structures—of the $R_mT_nX_p$ rare earth intermetallic compounds, where R is a rare earth atom, T is a d-electron atom and X is a p-electron atom. For these compounds the exchange interactions and the crystalline electric field are the two factors that influence the stability of the magnetic ordering of rare earth magnetic moments. Competition between these two interactions leads to a large variety of magnetic structures observed in ternary rare earth intermetallic compounds [1]. In this particular study we have investigated the $R_3Mn_4Sn_4$ (R = La, Pr, Nd) compounds, which crystallize in the orthorhombic $Gd_3Cu_4Ge_4$-type structure [2] (space group $Immm$, see figure 1). In this structure the rare earth atoms occupy two non-equivalent crystallographic positions. Bulk

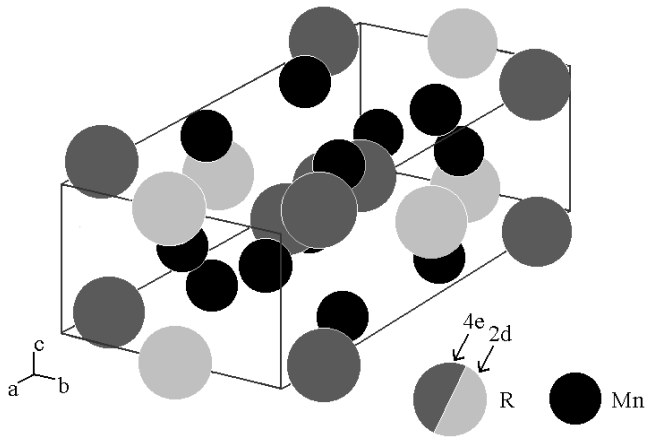

Figure 1. Crystal structure of the $R_3Mn_4Sn_4$ compounds. Only the R and Mn atoms are presented.

magnetic measurments indicated that these compounds are antiferromagnets with the Néel temperature equal to 16 K for R = Pr and to 45 K for R = Nd. In the case of $La_3Mn_4Sn_4$ the temperature dependence of the magnetic susceptibility has a broad maximum at about 300 K. For the temperature dependences of the magnetic susceptibilities of the Pr and Nd compounds no anomalies are observed close to room temperature [3]. The maxima of the magnetic susceptibility at 16 K for $Pr_3Mn_4Sn_4$ and 45 K for $Nd_3Mn_4Sn_4$ imply the onset of antiferromagnetic ordering at low temperatures. Above these temperatures the inverse magnetic susceptibility obeys the Curie–Weiss law in both compounds. These results suggest that in $La_3Mn_4Sn_4$ the Mn magnetic moments order at 300 K while in $Pr_3Mn_4Sn_4$ and $Nd_3Mn_4Sn_4$ probably only the rare earth moments order at low temperatures while the Mn moments do not. This contrasts the results for the RMn_2X_2 (X = Si, Ge) compounds, in which two regions with different magnetic properties exist: at low temperatures the magnetic moments of the rare earth and Mn atoms order while at high temperature only the Mn moments are ordered [4]. To clear up these conflicting results, neutron diffraction measurements as a function of temperature were performed. The paper reports the results of these investigations and the crystal and magnetic structure parameters of the examined $R_3Mn_4Sn_4$ (R = La, Pr, Nd) compounds are listed.

2. Experimental procedure

The polycrystalline samples, each with total weight of about 10 g, were synthesized by arc melting of stoichiometric amounts of 3 N for rare earth and Mn and 4 N purity for Sn elements in a Ti/Zr gettered argon atmosphere. The reaction products were annealed at 800 °C for a week. In order to check their purity, the samples were examined by x-ray powder diffraction (Cu Kα radiation). The peaks in the x-ray patterns were indexed in the orthorhombic $Gd_3Cu_4Ge_4$-type structure.

Neutron diffractograms were obtained using the E6 instrument at the BERII reactor, Hahn–Meitner Institut, Berlin. The incident neutron wavelength was 2.441 Å. The diffraction patterns were recorded at different temperatures between 1.5 K and room temperature. The Rietveld-type programme FULLPROF [5] was used to analyse the neutron diffraction data.

3. Symmetry analysis

Models used for refinement of magnetic structures are usually presented as sets of Fourier coefficients describing the magnetic moment components on particular ions. The use of symmetry is restricted to imposing extra constraints for magnetic moments localized on symmetry equivalent atoms. The method used here is based on the theory of representations of space groups and was first proposed by Bertaut [6] and Izyumov [7]. It gives the possibility to consider all the possible models for magnetic structures consistent with a given crystal structure with symmetry space group G. According to this method the magnetic structure given by $\boldsymbol{S}$ can be expressed in the coordinate system formed by the basic vectors $\Psi_\lambda^{k_l,\nu}$ of the irreducible representations of the group G. Such a coordinate system is the best one matching the symmetry of the problem and it provides the simplest form of the magnetic structure description because it requires the lowest number of independent parameters. $\boldsymbol{S}$ is described as a linear combination of basic vectors (magnetic modes) and given by

$$\boldsymbol{S} = \sum_{l,\nu,\lambda} c_\lambda^{k_l,\nu} \Psi_\lambda^{k_l,\nu} \tag{1}$$

where l is the number of $\boldsymbol{k}$-vectors determined by experiment, ν is the number of irreducible representations and λ the dimension of νth irreducible representations given by the symmetry of the crystal structure. The symmetry group $G(\boldsymbol{k})$ of the $\boldsymbol{k}$ vectors is a subgroup of the space group G. From this fact it follows that the sets of equivalent positions in the group G, the so-called orbits in G, may split into independent sets of equivalent positions in $G(\boldsymbol{k})$. Thus, one orbit in the group G can lead to two or more orbits in the $G(\boldsymbol{k})$ subgroup. The possible relations between the magnetic moments inside a given orbit are limited by symmetry and a single set of parameters describes the magnetic structure of all atoms belonging to the same orbit. Symmetry allows independent magnetic orderings on different orbits. For orbits belonging to different representations, the magnetic moments, phases etc differ and the magnetic moments localized at atoms belonging to one orbit may order at temperature T_1 while the moments belonging to another orbit order at T_2. The relations between the different orbits depend on the minimum of energy of the full structure, not on symmetry.

The form of the basic vectors and the information about which of the representations take part in the phase transition under consideration are directly given by the theory of groups and representations. In this work we use the computer programme MODY [8], which is based on the theory of groups and representations, to calculate this information. It is important to note that the basis vectors have the same translational properties as Bloch functions. Therefore, the basis vectors may be defined *on positions of given orbit* in the elementary cell of the crystal as well as in the elementary cell translated by a lattice vector $\boldsymbol{t}$, which just corresponds to a multiplication by $e^{i\boldsymbol{k}_l\boldsymbol{t}}$. The different sets of $c_\lambda^{k_l,\nu}$ parameters, where $c_\lambda^{k_l,\nu}$ may be complex, correspond to different models of the magnetic structure and may be used as good order parameters in the Landau–Ginzburg theory of phase transitions. However, not all of the possible $c_\lambda^{k_l,\nu}$ are allowed, because the parameters should be selected in such a way that the resulting magnetic moments related to all atoms have real values. This condition influences the set of equations which the $c_\lambda^{k_l,\nu}$ have to satisfy and as a result the number of independent free parameters is reduced and strictly determined. Because of the Bloch-like form of the basis vectors and the necessity of getting real values for $\boldsymbol{S}$, only one of the $\boldsymbol{k}$-vectors in the set of symmetry related $\boldsymbol{k}$-vectors (the so-called star of $\boldsymbol{k}$) has to be included in the linear combination for $\boldsymbol{S}$ (see equation (1)) if the magnetic cell is the same as the crystallographic unit cell or doubled in any direction ($k_i = 0$ or $\frac{1}{2}$). For any other commensurate or incommensurate magnetic structure both the $\boldsymbol{k}$ and $-\boldsymbol{k}$ vectors in the star of $\boldsymbol{k}$ must be included in a linear

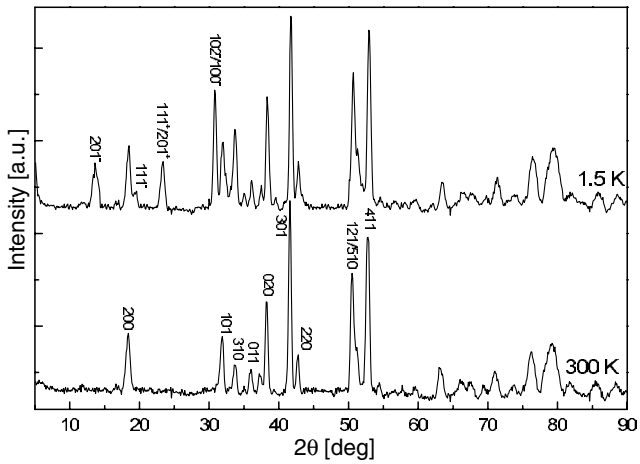

Figure 2. Neutron diffraction patterns of $La_3Mn_4Sn_4$ determined at 1.5 and 300 K.

combination describing $\boldsymbol{S}$. The essential fact is that magnetic phase transitions usually take place according to one irreducible representation with a not too large dimension.

The situation when the magnetic structure is described by basis vectors belonging to different irreducible representations indicates that the expression of the free energy of the structure cannot be limited only to the quadratic approximation. The free energy has the symmetry of a given space group, and therefore must be invariant under the action of this group. This means that the free energy transforms according to the identity representation of the given space group. Because the free energy may be presented as an nth-order polynomial of states, it may be written as a polynomial of products of the basic vectors of the irreducible representations used in the description of these states. It then follows from the theory of representations [7] that the products of basic vectors transform according to the direct product of representations to which these basic vectors belong. The direct product of representations is usually reducible and may be decomposed into irreducible representations. In the free energy only products of basic vectors, which include the identity representation in the decomposition, may appear. In the representation theory, it is proved that the second order product contains the identity representation only in the case when it is a product representation by itself. For this reason, it follows that the expression for the free energy the second order coupling between two states may appear only if these states belong to the same representation.

4. Results

4.1. Crystal structure

The neutron diffraction patterns recorded at 300 K for $La_3Mn_4Sn_4$ (see figure 2) and at 260 K for $Pr_3Mn_4Sn_4$ (figure 3) and $Nd_3Mn_4Sn_4$ (figure 4) confirmed that these compounds crystallize in the orthorhombic structure of the $Gd_3Cu_4Ge_4$ type described by the $Immm$ space group. The rare earth atoms occupy two sites: 2d ($\frac{1}{2}$, 0, $\frac{1}{2}$) and 4e (x, 0, 0). The Mn atoms are situated at the 8n (x, y, 0) sites and the Sn atoms are at 4f (x, $\frac{1}{2}$, 0) and 4h (0, y, $\frac{1}{2}$) sites in the crystal unit cell. The determined values of the lattice parameters a, b and c as well as the positional parameters corresponding to the minimum of the reliability factor are listed in table 1. The crystal structure of these compounds is shown in figure 1.

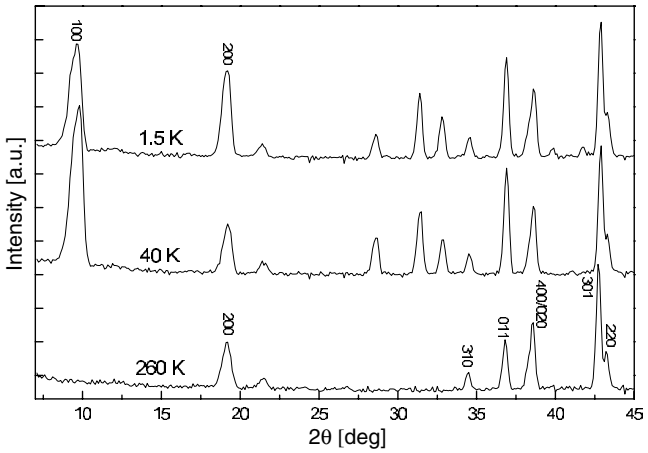

Figure 3. Neutron diffraction patterns of $Pr_3Mn_4Sn_4$ determined at 1.5, 40 and 260 K.

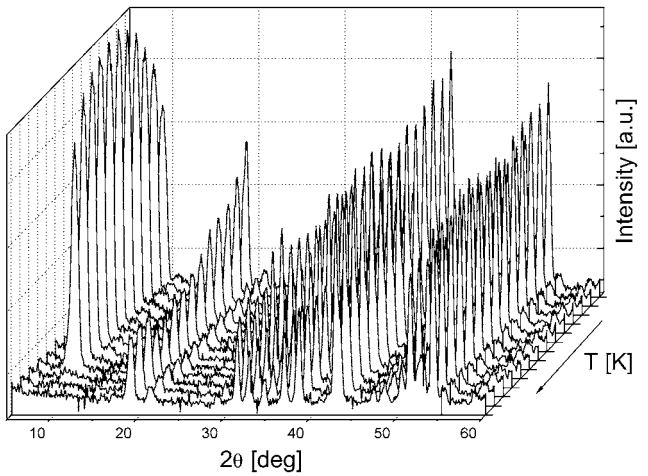

Figure 4. The temperature dependence of the $Nd_3Mn_4Sn_4$ neutron diffraction patterns measured in the temperature range 1.5–260 K (at 1.5, 20, 30, 35, 40, 45, 50, 55, 60, 120, 200, 220, 230, 240 and 260 K). The angular range (2θ) was from 5 to 60°.

4.2. Magnetic structure

The neutron diffraction patterns recorded at low temperatures reveal the presence of additional peaks of magnetic origin for all three compounds.

4.2.1. $La_3Mn_4Sn_4$. The additional peaks of magnetic origin that are observed in the neutron diffraction pattern at 1.5 K for $La_3Mn_4Sn_4$ (see figure 2) may be indexed with the propagation vector $\boldsymbol{k} = (k_x, 0, 0)$ where k_x is equal to 0.52 r.l.u. (r.l.u. stands for reciprocal length units). For this $\boldsymbol{k}$-vector the 8n crystallographic positions split into two independent orbits, $\boldsymbol{k}$ and $-\boldsymbol{k}$, of the $G(\boldsymbol{k})$ group. This means that the symmetry allows independent ordering of magnetic moments $\boldsymbol{S}$ and $\boldsymbol{S}'$ localized on atoms belonging to the two different orbits. The magnetic moments of the Mn atoms in the 8n sublattice occupy the following positions in the crystal unit

Table 1. The refined structural parameters of $La_3Mn_4Sn_4$, $Pr_3Mn_4Sn_4$ and $Nd_3Mn_4Sn_4$ (space group $Immm$ (no 71)). The standard deviations are given in brackets.

Compound	$La_3Mn_4Sn_4$	$Pr_3Mn_4Sn_4$	$Nd_3Mn_4Sn_4$
T (K)	300	260	260
a (Å)	15.291(5)	15.010(9)	14.962(7)
b (Å)	7.458(2)	7.451(4)	7.427(3)
c (Å)	4.661(1)	4.572(3)	4.551(2)
V (Å^3)	531.6(3)	511.3(5)	505.7(4)
x_R	0.1282(8)	0.123(3)	0.126(1)
x_{Mn}	0.333(1)	0.314(2)	0.328(2)
y_{Mn}	0.193(2)	0.171(4)	0.183(3)
x_{Sn}	0.2135(9)	0.227(2)	0.215(1)
y_{Sn}	0.196(2)	0.192(3)	0.207(2)
R_{Bragg} (%)	14.6	15.7	16.3
R_{prof} (%)	9.4	16.9	12.9

cell: $\boldsymbol{S}_1(x, y, 0)$, $\boldsymbol{S}_2(\bar{x}, \bar{y}, 0)$, $\boldsymbol{S}_3(\bar{x}, y, 0)$, $\boldsymbol{S}_4(x, \bar{y}, 0)$, $\boldsymbol{S}_5(\frac{1}{2}+x, \frac{1}{2}+y, \frac{1}{2})$, $\boldsymbol{S}_6(\frac{1}{2}-x, \frac{1}{2}-y, \frac{1}{2})$, $\boldsymbol{S}_7(\frac{1}{2}-x, \frac{1}{2}+y, \frac{1}{2})$, $\boldsymbol{S}_8(\frac{1}{2}+x, \frac{1}{2}-y, \frac{1}{2})$. The 1, 4, 5 and 8 moments belong to the first orbit whereas 2, 3, 6 and 7 moments to the second one. The proposed models for the magnetic orderings may be different for both orbits, and they should both be included in the model used to fit to the experimental diffraction pattern. For the $Immm$ group and $\boldsymbol{k} = (k_x, 0, 0)$ there are four one-dimensional irreducible representations. At the 8n positions the symmetry analysis allows two irreducible representations once (τ_1 and τ_4) and two irreducible representations twice (τ_2, τ_2' and τ_3, τ_3') for each orbit. The components of the basis vectors (e.g. the magnetic modes) of these irreducible representations are quoted in table 2. The symmetry analysis calculations show that for $La_3Mn_4Sn_4$ two independent parameters $-c^\nu$ and Φ^ν for the first orbit and d^ν and Θ^ν for the second orbit may describe all possible models of magnetic structures. The mixing coefficients in equation (1) are correspondingly $C_1^{k,\nu} = c^\nu e^{i\Phi^\nu}$, $C_1^{-k,\nu} = -c^\nu e^{i(\pi k_x - \Phi^\nu)}$, $C_1^{\prime k,\nu} = d^\nu e^{i\Theta^\nu}$, $C_1^{\prime -k,\nu} = -d^\nu e^{i(\pi k_x - \Theta^\nu)}$.

There are two two-dimensional magnetic phase transition order parameters, given by $p^\nu = (C_1^{k,\nu}, C_1^{-k,\nu})$ and $p'^\nu = (C_1^{\prime k,\nu}, C_1^{\prime -k,\nu})$, respectively. For this pair of free parameters the best fit to the experimental data is for the irreducible representations τ_3 [9] with $c^3 = d^3 = \mu_0 = 5.89(9)\ \mu_B$ and $\Delta = (\Theta^3 - \Phi^3) = 0.24\pi$. It is important to note that it is impossible to determine the absolute values of Θ^3 and Φ^3 from the diffraction patterns of polycrystalline samples, only the difference. This is in fact a global phase calibration preserving the phase differences between the two modes on the same ion and between various atoms.

The resulting magnetic structure may be written as

$$\boldsymbol{S}(1+\boldsymbol{t}) = \boldsymbol{S}(4+\boldsymbol{t}) = \mu_0 \boldsymbol{e}_y \cos(\boldsymbol{kt} + \Phi^3)$$
$$\boldsymbol{S}(5+\boldsymbol{t}) = \boldsymbol{S}(8+\boldsymbol{t}) = \mu_0 \boldsymbol{e}_y \cos(\boldsymbol{kt} + \pi k_x + \Phi^3)$$
$$\boldsymbol{S}(2+\boldsymbol{t}) = \boldsymbol{S}(3+\boldsymbol{t}) = \mu_0 \boldsymbol{e}_y \cos(\boldsymbol{kt} + \Theta^3)$$
$$\boldsymbol{S}(6+\boldsymbol{t}) = \boldsymbol{S}(7+\boldsymbol{t}) = \mu_0 \boldsymbol{e}_y \cos(\boldsymbol{kt} + \pi k_x + \Theta^3)$$

where $\boldsymbol{e}_y$ is the vector along the b-axis, $\boldsymbol{k}$ is the propagation vector and $\boldsymbol{t}$ the lattice translation vector.

The temperature dependences of the intensity of magnetic peaks shown in figure 5(b) suggest that the magnetic ordering is stable up to the Néel temperature, equal to 300 K. The value of the k_x component of the propagation vector increases with increasing temperature to the value of 0.61 r.l.u. at $T = 270$ K (see figure 5(a)).

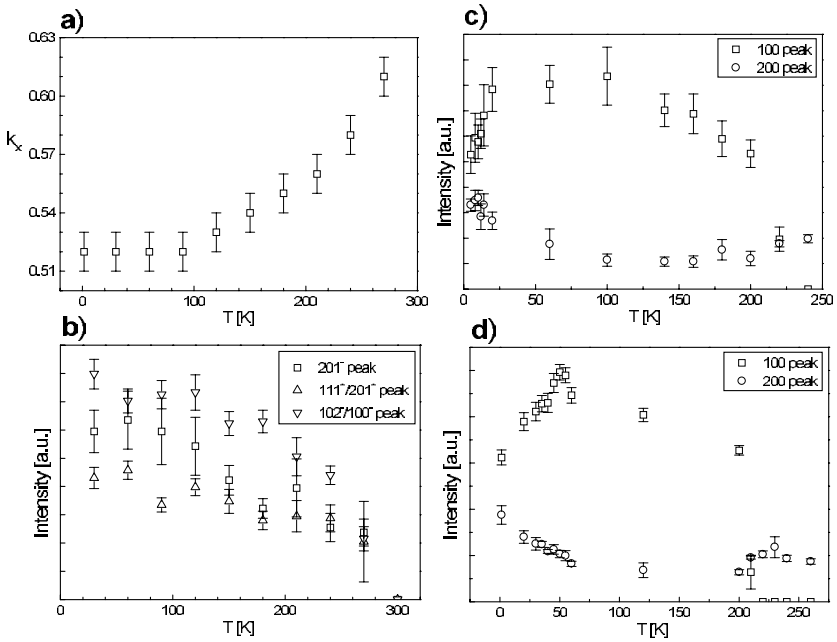

Figure 5. The temperature dependences of (a) the k_x component of the propagation vector for $La_3Mn_4n_4$, (b) the intensities of the 201^-, $111^+/201^+$ and $102^-/100^-$ magnetic Bragg peaks for $La_3Mn_4Sn_4$, (c) the 100 and 200 magnetic Bragg peaks for $Pr_3Mn_4Sn_4$ and (d) those for $Nd_3Mn_4Sn_4$.

4.2.2. $Pr_3Mn_4Sn_4$. On the neutron diffraction pattern of $Pr_3Mn_4Sn_4$ the additional peaks of magnetic origin are observed at 1.5 K (see figure 3). These peaks could be indexed in the conventional crystal unit cell but with antiferromagnetic coupling of atoms related by the $(\frac{1}{2}\frac{1}{2}\frac{1}{2})$ centring translations corresponding to the magnetic propagation vector $\boldsymbol{k} = (1, 1, 1)$. The Pr magnetic moments occupy two sites with the following positions in the crystal unit cell:

- 4e sites: $\boldsymbol{S}_1(x, 0, 0)$, $\boldsymbol{S}_2(\bar{x}, 0, 0)$, $\boldsymbol{S}_3(\frac{1}{2}+x, \frac{1}{2}, \frac{1}{2})$, $\boldsymbol{S}_4(\frac{1}{2}-x, \frac{1}{2}, \frac{1}{2})$ and
- 2d sites: $\boldsymbol{S}_5(\frac{1}{2}, 0, \frac{1}{2})$, $\boldsymbol{S}_6(0, \frac{1}{2}, 0)$.

The temperature dependence of the intensities of the 100 and 200 reflections (see figure 5(c)) reveals that with increasing temperature the magnetic structure changes.

For the $Immm$ space group and vector $\boldsymbol{k} = (1, 1, 1)$ the 4e and 8n sites each form one orbit of the $G(\boldsymbol{k})$ group. For the 4e case the symmetry analysis shows that six one-dimensional irreducible representations are admissible—each of them only once. For the 8n positions eight one-dimensional irreducible representations are admissible—four of them twice. Because the magnetic cell is the same as the crystallographic cell, only one $\boldsymbol{k}$-vector has to be taken into account in the linear combination in equation (1) for getting the magnetic structure models. Each magnetic structure model may be described by the basis vector of the corresponding irreducible representation and one free parameter $C_1^{k,\nu} = \mu_i$, which represents the magnitude of the ith magnetic moment. The components of the basis vectors (e.g. the magnetic modes) of the irreducible representations for vector $\boldsymbol{k} = (1, 1, 1)$ for the 4e sites are quoted in table 3 and the corresponding ones for the 8n sites are quoted in table 4.

Table 2. Basic vectors of the irreducible representations for $\boldsymbol{k} = (k_x, 0, 0)$ of the $Immm$ space group in the 8n positions. The magnetic modes related to the moments on sites 5, 8 and 6, 7 are the modes for sites 1, 4 and 2, 3, respectively, multiplied by $e^{i\phi}$ for $\boldsymbol{k}$ and $e^{-i\phi}$ for $-\boldsymbol{k}$, where $\phi = \pi k_x$.

		$(x, y, 0)$	$(\bar{x}, \bar{y}, 0)$	$(\bar{x}, y, 0)$	$(x, \bar{y}, 0)$
$\boldsymbol{k}$					
τ_1	1st orbit	(0, 0, 1)			(0, 0, −1)
	2nd orbit		(0, 0, −1)	(0, 0, 1)	
τ_2	1st orbit	(1, 0, 0)			(1, 0, 0)
	2nd orbit		(1, 0, 0)	(1, 0, 0)	
τ_2'	1st orbit	(0, 1, 0)			(0, −1, 0)
	2nd orbit		(0, −1, 0)	(0, 1, 0)	
τ_3	1st orbit	(0, 1, 0)			(0, 1, 0)
	2nd orbit		(0, 1, 0)	(0, 1, 0)	
τ_3'	1st orbit	(1, 0, 0)			(−1, 0, 0)
	2nd orbit		(1, 0, 0)	(−1, 0, 0)	
τ_4	1st orbit	(0, 0, 1)			(0, 0, 1)
	2nd orbit		(0, 0, 1)	(0, 0, 1)	
$-\boldsymbol{k}$					
τ_1	1st orbit	$(0, 0, e^{-i\phi})$			$(0, 0, -e^{-i\phi})$
	2nd orbit		$(0, 0, -e^{-i\phi})$	$(0, 0, e^{-i\phi})$	
τ_2	1st orbit	$(e^{-i\phi}, 0, 0)$			$(e^{-i\phi}, 0, 0)$
	2nd orbit		$(e^{-i\phi}, 0, 0)$	$(e^{-i\phi}, 0, 0)$	
τ_2'	1st orbit	$(0, -e^{-i\phi}, 0)$			$(0, e^{-i\phi}, 0)$
	2nd orbit		$(0, e^{-i\phi}, 0)$	$(0, -e^{-i\phi}, 0)$	
τ_3	1st orbit	$(0, -e^{-i\phi}, 0)$			$(0, -e^{-i\phi}, 0)$
	2nd orbit		$(0, -e^{-i\phi}, 0)$	$(0, -e^{-i\phi}, 0)$	
τ_3'	1st orbit	$(e^{-i\phi}, 0, 0)$			$(-e^{-i\phi}, 0, 0)$
	2nd orbit		$(e^{-i\phi}, 0, 0)$	$(-e^{-i\phi}, 0, 0)$	
τ_4	1st orbit	$(0, 0, e^{-i\phi})$			$(0, 0, e^{-i\phi})$
	2nd orbit		$(0, 0, e^{-i\phi})$	$(0, 0, e^{-i\phi})$	

The analysis of the magnetic peak intensities indicates that at 1.5 K the 4e Pr moments are ordered in the xy-plane and form a collinear, antiferromagnetic structure with the sign sequence $--++$ for the x-component and $++--$ for the y-component ($\mu_x = -2.8(1)\ \mu_B$ and $\mu_y = 0.5(2)\ \mu_B$). The amplitude of the Pr moment is equal to $2.9(2)\ \mu_B$ and is smaller than the free Pr^{3+} ion value ($3.2\ \mu_B$). Two basis vectors belonging to two different irreducible representations describe the above-mentioned magnetic structure. They are τ_3 for the x-component and τ_5 for the y-component—as may be seen from table 3. The Pr magnetic moments at 2d sites are not ordered. The diffraction patterns also show that the Mn moments are ordered in the zy-plane and form a non-collinear, antiferromagnetic structure with the sign sequence $+--+-++-$ for the z-component (with $\mu_z = 1.31(5)\ \mu_B$), and $++++----$ for the y-component ($\mu_y = 1.91(1)\ \mu_B$). The amplitude of the Mn magnetic moment is equal to $2.3(1)\ \mu_B$. As is the case for the Pr atoms, two basis vectors belonging to two different irreducible representations describe this ordering. They are τ_6 for the z-component and τ_5 for the y-component listed in table 4. Such a situation means that the expression of the free energy of this structure cannot be limited only to the quadratic approximation, and indicates higher order couplings between different components of the magnetic moments. Near 25 K the 4e Pr moments disorder but the ordering of the Mn moments remains similar to the magnetic structure observed at 1.5 K up to the Néel temperature of 230 K. The refinement of the magnetic peak intensities at 40 K yields $\mu_z = 1.50(5)\ \mu_B$, $\mu_y = 2.2(1)\ \mu_B$ and the amplitude of the Pr magnetic moment of $2.7(1)\ \mu_B$.

Table 3. Basic vectors of the irreducible representations $\boldsymbol{k} = (1, 1, 1)$ of the $Immm$ space group in the 4e positions; $\boldsymbol{S}(3, 4) = -\boldsymbol{S}(1, 2)$.

	$(x, 0, 0)$	$(\bar{x}, 0, 0)$
τ_2	(1, 0, 0)	(−1, 0, 0)
τ_3	(1, 0, 0)	(1, 0, 0)
τ_5	(0, 1, 0)	(0, 1, 0)
τ_6	(0, 0, 1)	(0, 0, −1)
τ_7	(0, 0, 1)	(0, 0, 1)
τ_8	(0, 1, 0)	(0, −1, 0)

Table 4. Basic vectors of the irreducible representations $\boldsymbol{k} = (1, 1, 1)$ of the $Immm$ space group in the 8n positions; $\boldsymbol{S}(5, 6, 7, 8) = -\boldsymbol{S}(1, 2, 3, 4)$.

	$(x, y, 0)$	$(\bar{x}, \bar{y}, 0)$	$(\bar{x}, y, 0)$	$(x, \bar{y}, 0)$
τ_1	(0, 0, 1)	(0, 0, 1)	(0, 0, −1)	(0, 0, −1)
τ_2	(1, 0, 0)	(−1, 0, 0)	(−1, 0, 0)	(1, 0, 0)
τ_2'	(0, 1, 0)	(0, −1, 0)	(0, 1, 0)	(0, −1, 0)
τ_3	(1, 0, 0)	(1, 0, 0)	(1, 0, 0)	(1, 0, 0)
τ_3'	(0, 1, 0)	(0, 1, 0)	(0, −1, 0)	(0, −1, 0)
τ_4	(0, 0, 1)	(0, 0, −1)	(0, 0, 1)	(0, 0, −1)
τ_5	(1, 0, 0)	(1, 0, 0)	(−1, 0, 0)	(−1, 0, 0)
τ_5'	(0, 1, 0)	(0, 1, 0)	(0, 1, 0)	(0, 1, 0)
τ_6	(0, 0, 1)	(0, 0, −1)	(0, 0, −1)	(0, 0, 1)
τ_7	(0, 0, 1)	(0, 0, 1)	(0, 0, 1)	(0, 0, 1)
τ_8	(1, 0, 0)	(−1, 0, 0)	(1, 0, 0)	(−1, 0, 0)
τ_8'	(0, 1, 0)	(0, −1, 0)	(0, −1, 0)	(0, 1, 0)

4.2.3. $Nd_3Mn_4Sn_4$. The neutron diffraction pattern of $Nd_3Mn_4Sn_4$ at 1.5 K is similar to the one observed for $Pr_3Mn_4Sn_4$ (see figure 4). All peaks of magnetic origin are indexed as the ones for the conventional crystal unit cell. The magnetic structure at 1.5 K is similar to that observed in $Pr_3Mn_4Sn_4$:

- the Nd moments in the 2d sites do not order;
- the Nd moments in the 4e sites form a collinear structure with $\mu_x = -2.6(1)\ \mu_B$, $\mu_y = 1.4(1)\ \mu_B$ and $\mu_{total} = 3.0(1)\ \mu_B$ and
- the Mn moments in the 8n sites form a non-collinear structure with $\mu_y = 2.80(7)\ \mu_B$, $\mu_z = 1.53(4)\ \mu_B$ and $\mu_{total} = 3.20(6)\ \mu_B$.

In the temperature range 60–200 K magnetic moment is localized only on the Mn atoms and forms a non-collinear structure similar to that observed in $Pr_3Mn_4Sn_4$ with 2.88(7) μ_B for the y-component and 1.39(5) μ_B for the z-component at 60 K. The value of the amplitude of the Mn moment decreases with the temperature from 3.2(1) μ_B at 60 K to 2.8(1) μ_B at 200 K. At $T = 210$ K a sharp jump of the intensity of the magnetic 100 peak is observed (see figure 5(d)).

Figure 6 shows the temperature dependences of the lattice parameters a, b and c and the unit cell volume V of $Nd_3Mn_4Sn_4$. The temperature dependences of all lattice parameters and the unit cell volume have minima at T_t equal to 60 K when the Nd moments order. Below T_t the values of all these parameters increase with decreasing temperature. This result indicates a positive sign of the magnetostriction. At the Néel temperature $T_N = 210$ K jumps in all of the lattice parameters a, b and c and of the unit cell volume V are observed. The magnetostriction of all lattice parameters and the unit cell volume is negative at this magnetic

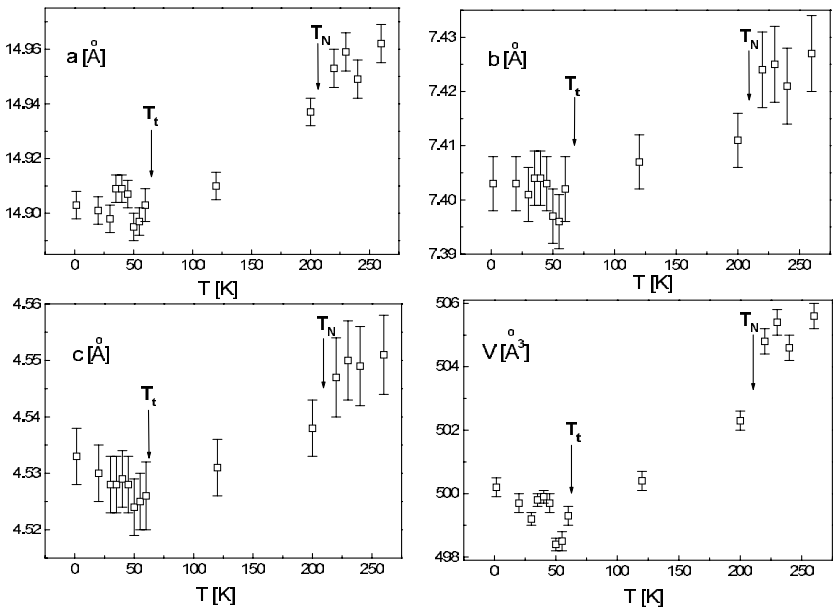

Figure 6. Temperature dependence of the lattice parameters a, b and c and the volume of the unit cell V in $Nd_3Mn_4Sn_4$.

phase transition. These results for $Nd_3Mn_4Sn_4$ are consistent with those observed in the RMn_2X_2 compounds [10].

5. Discussion

The results obtained in this investigation show that the $R_3Mn_4Sn_4$ (R = La, Pr, Nd) compounds have complex magnetic properties. In $La_3Mn_4Sn_4$ the Mn magnetic moments form a sine wave modulated structure below the Néel temperature. The magnetic moment is parallel to the b-axis and its amplitude is equal to 5.89(9) μ_B. The magnetic moment at the atom position $\boldsymbol{r}$ is given by $\mu(\boldsymbol{r}) = \frac{\pi}{4}\mu(\boldsymbol{k}) = 4.63(7)\ \mu_B$. The value of the Néel temperature (300 K) determined from the neutron diffraction data is in a good agreement with the magnetic data reported in [3].

Somewhat more complex magnetic orderings are observed for $Pr_3Mn_4Sn_4$ and $Nd_3Mn_4Sn_4$. Below the Néel temperature (230 K for $Pr_3Mn_4Sn_4$ and 210 K for $Nd_3Mn_4Sn_4$) the Mn moments form a non-collinear magnetic structure. At low temperatures, below 25 K for $Pr_3Mn_4Sn_4$ and 60 K for $Nd_3Mn_4Sn_4$, the rare earth moments in the 4e sites form collinear antiferromagnetic structures. Similar relations between the temperature of the ordering of the magnetic moments in Mn and rare earth sublattices are observed in RT_2X_2 compounds [4].

The $R_3Mn_4Sn_4$ (R = La, Pr, Nd) compounds investigated in this work crystallize in a complicated crystal structure. The interatomic distances between the atoms calculated on the basis of the crystal structure parameters listed in table 1 are presented in table 5. In all the three $R_3Mn_4Sn_4$ compounds the rare earth interatomic distances between the atoms at the 2d and 4e sites and between the rare earth moments at the 2d sites are rather large. This may mean that the couplings between the rare earth moments at these sites are weaker than in the related compounds and thus explain the absence of the ordering between the rare earth moments at the 2d sites.

The Mn–Mn distance is smaller. For the Pr and Nd compounds the Mn–Mn distances ($d_{\mathrm{Mn-Mn}}$) are smaller than the critical Mn–Mn distances ($d_c = 2.85$ Å) observed in the RMn_2X_2

Table 5. The interatomic distances in $R_3Mn_4Sn_4$ (R = La, Pr, Nd) compounds given in Å.

	$La_3Mn_4Sn_4$	$Pr_3Mn_4Sn_4$	$Nd_3Mn_4Sn_4$
R(4e)–R(4e)	3.92	3.77	3.69
R(2d)–R(2d)	7.458	7.427	7.451
R(2d)–R(4e)	4.213	4.158	4.165
R(2d)–Sn(4h)	3.251	3.239	3.149
R(2d)–Sn(4f)	3.265	3.407	3.217
R(4e)–Mn	3.320	3.137	3.313
R(4e)–Mn	3.446	3.446	3.346
R(4e)–Sn(4h)	3.378	3.268	3.331
R(4e)–Sn(4f)	3.360	3.209	3.292
R(4e)–Sn(4f)	3.950	4.039	3.945
Mn–Mn (in-plane)	2.879	2.748	2.718
Mn–Mn (out-of-plane)	3.549	3.210	3.408
Mn–Sn(4h)	2.684	2.973	2.700
Mn–Sn(4f)	2.929	2.777	2.898
Mn–Sn(4f)	2.830	2.688	2.727

(X = Si, Ge) compounds. In the RMn_2Ge_2 compounds the antiferromagnetic state appears for $d_{Mn-Mn} < 2.85$ Å and the ferromagnetic state for $d_{Mn-Mn} > 2.85$ Å [1]. Similar critical distances were observed in many alloys containing transition metals [11, 12]. Goodenough [13] suggested that the localization–delocalization effect of the 3d electrons occurs when the critical distance in the Mn compounds is 2.85 Å. The Mn–Mn distance in $La_3Mn_4Sn_4$ is slightly larger than the critical value. In the compounds investigated in this paper the observed dependence of the Néel temperature value decreases with the decrease of the Mn–Mn distance. This result is opposite to the results for the RMn_2X_2 (X = Si, Ge) where the Néel temperature decreases with increasing Mn–Mn distances (see figure 32 in [14]).

In the temperature dependences of the intensity of the magnetic 200 peak and the Mn magnetic moment value for $Nd_3Mn_4Sn_4$ (see figure 5(d)) a sharp jump at the Néel temperature is observed. This suggests that the phase transition at the Néel temperature is of first order. Such a phase transition is accompanied by negative magnetostriction (see figure 6).

Acknowledgments

This work was partially supported by the European Commission under the Access to Research Infrastructures of the Human Potential Programme (contract number HPRI-CT-1999-00020) and by the State Committee for Scientific Research in Poland (grant number 2 PO3B 113 23). The authors (SB, JL and AS) would like to express their gratitude to the management of the Berlin Neutron Scattering Centre for financial support and kind hospitality.

References

[1] Szytuła A and Leciejewicz J 1994 *Handbook of Crystal Structure and Magnetic Properties of Rare Earth Intermetallics* (Boca Raton, FL: Chemical Rubber Company Press)
[2] Rieger W 1970 *Monat. Chem.* **101** 449
[3] Weitzer F, Hiebl K, Rogl P and Noël H 1992 Crystal chemistry and magnetic behaviour of compounds $RE_3Mn_4Sn_4$, R = La, Ce, Pr, Nd, Sm and MM (Mischmetal) *Ber. Bunsenges. Phys. Chem.* **96**
[4] Szytuła A and Leciejewicz J 1989 *Handbook on Physics and Chemistry of Rare Earths* vol 12, ed K A Gschneider Jr and L Eyring (Amsterdam: Elsevier) ch 83 p 133
[5] Rodriguez-Carvajal J 1993 *Physica* B **192** 55

[6] Bertaut E F 1968 *Acta Crystallogr.* A **24** 217
[7] Izyumov Y A 1990 *Phase Transitions and Crystal Symmetry* (Dordrecht: Kluwer)
[8] Sikora W 1994 *Proc. Symmetry and Structural Properties of Condensed Matter (Zajączkowo, Poland)* p 484
[9] Kovalev O V 1993 *Representations of the Crystallographic Space Groups* ed H T Stokes and D M Hatch (London: Gordon and Breach)
[10] Shigeoka T 1984 *J. Sci. Hiroshima Univ.* A **48** 103
[11] Tabble R S and Craik D J 1969 *Magnetic Materials* (New York: Wiley) p 61
[12] Forrer R 1952 *Ann. Phys., NY* **7** 605
[13] Goodenough J B 1963 *Magnetism and Chemical Bond* (New York: Wiley) p 240
[14] Szytuła A 1991 *Handbook of Magnetic Materials* vol 6, ed K H J Buschow (Amsterdam: Elsevier) ch 2 p 85